J. Fluid Mech. (1993), *vol.* 251, *pp.* 581–601

An experimental study of laminar plumes

By ELISHA MOSES† GIOVANNI ZOCCHI‡ AND ALBERT LIBCHABER‖

The James Franck and Enrico Fermi Institutes, The University of Chicago, 5640 S. Ellis Ave., Chicago, IL 60637, USA

(Received 15 January 1991 and in revised form 18 December 1992)

We present an experimental study of the scaling laws for the front (or cap) of an isolated, laminar starting plume. The scaling relations are formulated and measured experimentally over a range of power, fluids, and heaters. The results are that the cap rises at constant velocity, grows diffusively in width, and its temperature depends inversely on height. This extends analytic results by Batchelor (1954) for the column (stem) below the front. The source size determines initial conditions for the cap, but does not affect it in the far field. The shape of the front is fitted by a model of potential flow. The interaction between plume caps is complex, but with simple underlying dynamics. We conjecture that some of our conclusions can be applied to a distribution of plumes, as in soft turbulent convection.

1. Introduction

When a heat flux is applied to a localized region in a fluid, the ensuing mushroom-like convection pattern has three main constituents: a boundary layer in the vicinity of the heater; a cap which forms at the upwards propagating front; and a corridor (or stem) connecting the two (see insert to figure 1). In practical situations the relevant structure is usually the stem, since in heat transfer the problem is the long-term cooling, and transient phenomena are unimportant. However, in the study of turbulent convection it has been found (Chu & Goldstein 1973; Solomon & Gollub 1990; Zocchi, Moses & Libchaber 1990) that at moderately high Rayleigh numbers the caps become the dominant structures in the flow field. It is for this reason that we developed an interest in the behaviour of the caps themselves.

It is our aim in this paper to present the scaling laws of the cap (see table 1). For that purpose, we first formulate the equations of motion with realistic boundary conditions, then experimentally measure the scaling exponents for (i) the rising velocity of the cap, (ii) the growth rate of the cap, and (iii) the temperature inside the cap. The results can be summarized by saying that the velocity is constant in time and scales with power input and viscosity (figure 4), the growth rate is diffusive (figure 6), and the temperature scales inversely with height and directly with power input (figure 7). We present results on the shape of the plume and on the transient leading to its formation. The stem is treated only in passing. Interactions (and collisions) between plumes are a natural extension of this study, and we find that simple dynamics can describe them. We also give arguments that the scaling laws may be valid for plumes in some range of convective turbulence.

† Present address: Department of Physics, Weizmann Institute, Rehovot 76100, Israel.
‡ Present address: Ecole Normale Superieure, 24 rue Lhomond, 75005 Paris, France.
‖ Present address: Department of Physics, Princeton University, Princeton, NJ 08544, USA.

Quantity	Prefactor	Batchelor variables	Non-dimensional variables	Dimensional variables
Velocity v_c	(0.20 ± 0.02)	$(F/\nu)^{\frac{1}{3}}$	$\frac{\kappa}{R}\mathscr{R}_f^{\frac{1}{3}}\sigma^{-\frac{1}{3}}$	$\left(\frac{g\alpha P}{\nu\rho C_p}\right)^{\frac{1}{3}}$
Cap width $a-a_0$	(4.2 ± 0.2)	$\sigma^{-\frac{1}{3}}\left(\frac{\nu^3}{F}\right)^{\frac{1}{4}}z^{\frac{1}{2}}$	$R\left(\frac{t-t_0}{\tau}\right)^{\frac{1}{2}}$	$[\kappa(t-t_0)]^{\frac{1}{2}}$
Build-up time t_0	(40 ± 5)	$\left(\frac{\nu}{F}\right)^{\frac{1}{3}}R$	$\frac{R^2}{\kappa}\mathscr{R}_f^{-\frac{1}{3}}\sigma^{\frac{1}{3}}$	$\left(\frac{\nu\rho C_p R^2}{g\alpha P}\right)^{\frac{1}{3}}$
Cap temperature θ	(0.05 ± 0.01)	$\sigma\frac{F}{g\alpha\nu}z^{-1}$	$\chi\frac{R}{z}$	$\frac{P}{\kappa\rho C_p z}$

TABLE 1. Summary of the scaling relations determined experimentally. Here $F = g\alpha P/\rho C_p$ is Batchelor's scaling variable, $\mathscr{R}_f = g\alpha P R^2/\kappa^3\rho C_p$ our version of the flux Rayleigh number, and $\sigma = \nu/\kappa$ is the Prandtl number.

2. Review of previous results

Much effort has been devoted to the study of plumes and in reviewing the literature one finds diversity and some confusion. This comes from the fact that plumes may originate from a point or a line source, can have a sustained or 'one-shot' heat input (thermals), can be steady (the stem) or starting (the cap), can be turbulent or laminar, and thus a unified view is hard to come by. For a review on the subject see, e.g. Turner (1969, 1973, chap. 6.) and Gebhart *et al.* (1988).

The related subject of a point source of intense heat became the object of obvious attention with the advent of the atomic bomb, and was treated by Taylor (1941, 1950*a*, *b*) and by von Neumann (1941, 1946). In that case, a shock wave develops and the only length scales with $t^{\frac{2}{5}}$ (t is time).

Plumes are slightly more complex, combining effects of buoyancy, diffusion and advection. It seems that Zeldovich (1937) was the first to treat the steady-state problem of the stem. A clear outline and the main results are given by Batchelor (1954). A similarity solution of the form $z^m f(r/a)$ for the velocity and the temperature inside the stem is assumed, where z is the height, r the radial distance, a the radius of the plume and f an unspecified profile function. Dimensional analysis then invokes heat conservation along the stem and assumes a balance between viscous dissipation and buoyancy forces. The result is that the vertical velocity v_s is constant, the lateral growth is governed by diffusion processes, so that the stem's shape is parabolic, and the temperature is linear with heat input and inversely proportional to height, which implies that the Nusselt number is constant.

On the basis of these results, analytical solutions for the stem in the laminar case, using a similarity approach, have been given by Yih (1951), Fujii (1963), Fujii, Morioka & Uehara (1973) and Pera & Gebhart (1971). They all found an analytical solution for a two-dimensional approximation of the problem at special values of the control parameters (e.g. Prandtl numbers of 1 and 2). They did not give a scaling dependence on the Prandtl number, and for different values of this parameter a numerical technique was needed.

The cap itself was first treated theoretically by Turner (1962), building on his work with Taylor and Morton (see below). He matched a vortex ring solution on top of a

turbulent stem solution. As a result, the cap velocity v_c decreased with height ($v_c \sim z^{-\frac{1}{3}}$) and the width was linear with height. This scaling is different from the measurements of laminar starting plumes reported in the present paper, since it corresponds to a turbulent stem. We shall show that in a way Turner's result is also valid for the laminar case, in the sense that the scaling established in the stem extends into the cap.

Plumes lose their stability when the Reynolds number of the cap becomes too big. For turbulent plumes advective processes are dominant, and diffusive ones irrelevant. Lateral growth of the stem when advection dominates can occur only by entrainment from the surrounding fluid. For a discussion of the entrainment assumption and its consequences, see Turner (1986). The horizontal inflow velocity is shown to be proportional to the vertical velocity, which is no longer constant, decreasing with height. The lateral expansion is proportional to the height, and the shape of the stem is then conical. Morton, Taylor & Turner (1956) quantified the effect of entrainment, and formulated a model that generalized these results for the atmosphere, where the surrounding fluid is stratified.

On the experimental side, very extensive work has been done by Gebhart and coworkers on the properties of the stem (see e.g. Schorr & Gebhart 1970; Gebhart, Pera & Schorr 1970; Pera & Gebhart 1975 and Polymeropoulos & Gebhart 1967). The configuration of choice was usually a linear heater, which is the practical situation (cooling from a hot pipe) and is experimentally convenient. The temperature field was measured by an interferometric technique. A comprehensive account can be found in the book by Gebhart *et al.* (1988).

The most extensive experimental study of the cap has been done by Shlien and coworkers. Shlien & Boxman (1979) have measured the temperature field inside the steady-state stem, comparing it to the analytic similarity solutions of Yih, but had to postulate the existence of a virtual point source to obtain agreement. They also measured the detailed temperature field in the cap (Shlien & Boxman 1981), while Shlien & Brosh (1979) measured the velocity field inside a one-shot plume (thermal). Since the existing similarity theory was derived for the temperature of the stem, not of the cap, they did not check its scaling properties. Scaling results were given for the rise velocity of the cap (Shlien 1979), but again, since no theory was available, they measured only the obvious parameter of power input. Shlien (1976) did try to measure the scaling of the width of the cap, but he had a limited resolution, and since the only scaling theory at his disposal was Turner's, he ended up concluding that the cap size is proportional to the height. This is different from the scaling that we measure. Shlien (1978) gave a criterion for destabilization of the plume that depends on the Reynolds number at the cap.

Plumes also appear in other circumstances: Sparrow, Husar & Goldstein (1970) showed by using an electrochemical dye that many plumes are created above a heated horizontal plate, and that they appear with a periodicity related to the time for creation of a thermal boundary layer. Chu & Goldstein (1973) discovered starting plumes in a visualization experiment on turbulent convection, which sparked a renewed interest in these structures. More recently, experiments on turbulent convection by Solomon & Gollub (1990) and by Zocchi *et al.* (1990) using thermochromic liquid crystals have shown that the plumes are part of a cycle of coherent structures that comprise the large-scale turbulent flow.

3. The experimental apparatus

Our experimental apparatus consists of a glass tank $10 \times 10 \times 20$ cm high. Temperature stability over the lifetime of the plumes was typically better than 5 mK. Typical heaters were 100 Ω commercial resistors. For cylindrical heaters we defined an effective radius R as the radius of a sphere with the same surface area. We used three cylinders of length 0.3, 0.5 and 1.8 cm with $R = 0.06$, 0.17 and 0.58 cm respectively, and spherical heaters of radius 2–4 mm made by embedding a heater inside a brass or copper ball. We monitored the internal temperature of the 100 Ω, $R = 0.17$ cm resistor by embedding inside it a thermistor, whose resistance we monitored. The smallest heater used ($R = 0.06$) was a commercial thermistor, and by monitoring its own resistance we knew the temperature inside it.

The bulk of our measurements utilized a standard computer-enhanced shadowgraph technique. Our resolution, in space, was about 0.5 mm, and in time was 30 Hz. We periodically checked the geometrical distortion by the calibration of known lengths, keeping distortion below 5%. The distortion due to the shadowgraph is harder to evaluate, since the nonlinear effects are difficult to calibrate. The plume presents a problem both because it is an imperfect lens and because its effective focal length changes as it rises, by growing and by cooling. For large enough deflection of the rays from the source a caustic is formed outside the plume – this occurs in water near the heater, and in oil all along the plume. At lower density gradients a thin 'halo' forms round the heated regions.

We therefore checked the shadowgraph against a visualization technique utilizing thermochromic liquid crystals (TLC). These are commercial cholesteric liquid crystals (manufactured by Hallcrest of Glenview, IL) encapsulated in microspheres (50–100 μm diameter). In very low concentrations ($\sim 10^{-4}$ by weight) they behave in the flow as suspensions. One obtains a qualitative picture of the temperature field (through the colour change of the liquid crystals), and also of the velocity field (by following the motion of the particles). The colour turns from red to green to blue in a temperature window of about 1 °C around 25 °C. An example of this visualization is shown in figure 1.

By comparing these two techniques we found that the shadowgraph obscures the edge of the temperature profile, where the gradients are small and the temperature slowly falls off. The stem entrains colder fluid into its envelope, but the core remains hot. Thus in the shadowgraph we see the stem as an essentially straight black column. The TLC picks up the full extent of the stem, showing it to widen as it rises. For the cap we found that TLC gives the same shape as that given by the shadowgraph, but slightly larger – in the white border on top of the shadowgraph image of the cap there is region of intermediate heat, which the shadowgraph misses because it is near the region of large gradient.

We measured the temperature of the cap by placing a thermistor in its path. This was sensitive to the intricate structure inside the cap and to lateral deviations in the plume trajectory, with a scatter of 10% typical. Only the initial climb of the temperature as the plume cap hits the heater was used.

To explore a wide span of the control parameters we used a variety of fluids. Table 2 summarizes the physical properties for the fluids we used. We found that the data provided for the oils is correct to within 10–15%. The viscosities of the oils have an exponential dependence on temperature, but our measurements are not affected by this, either because viscosity does not figure in the quantity measured, or because the relevant viscosity is that of the ambient, not the heated, fluid.

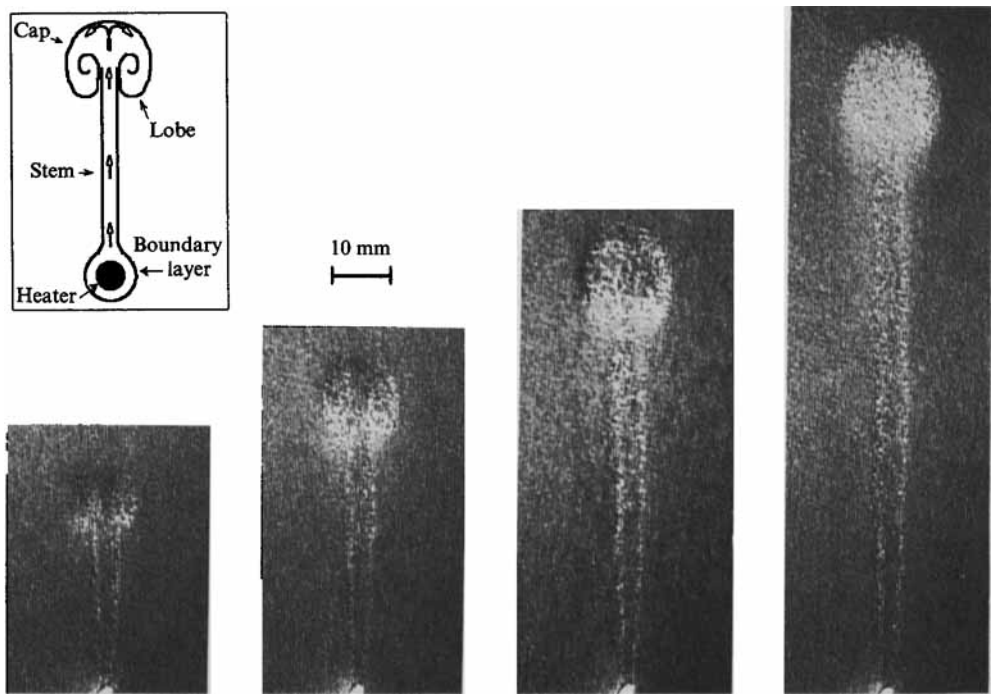

(*a*) (*b*) (*c*) (*d*)

FIGURE 1. Thermochromic liquid crystals used to visualize a rising plume. A vertical sheet of white light ~ 2 mm thick is shone from the left. $P = 1.25$ W, $R = 0.17$ cm, $t_0/\tau = 0.12$. Shades of green and blue (hot) are seen as light areas, while the red (colder) background is dark. The heater is bright white at bottom centre. Non-dimensional time t/τ is (*a*) 0.47, (*b*) 0.61, (*c*) 0.77, (*d*) 1.02. Insert: schematic drawing of a plume, illustrating its major constituents. Arrows inside the plume indicate the flow along the stem and into the cap.

	Water	Methanol	Pump oil	Silicon oil
Density, ρ (g/cm^3)	0.997	0.787	0.81	1.11
Viscosity, ν (cm^2/s)	8.9×10^{-3}	7×10^{-3}	0.3	5.0
Thermal diffusivity, κ (cm^2/s)	1.45×10^{-3}	1.0×10^{-3}	8×10^{-4}	9×10^{-4}
Specific heat, C_p (J/g K)	4.18	2.5	2.3	1.5
Expansion coefficient, α (1/K)	2.6×10^{-4}	1.4×10^{-3}	7×10^{-4}	8×10^{-4}
Prandtl number, σ	6.2	7	3.8×10^{2}	5.7×10^{3}

TABLE 2. Physical properties at 25 °C of the fluids used in the experiment. The pump oil used was Precision D manufactured by the GCA Precision Scientific Group, Chicago IL, and the silicon oil was Dow Corning 710 Fluid manufactured by the Dow Corning Corp., Midland, MI.

4. The scaling approach

The equations for this system (in the Oberbeck–Boussinesq approximation) are

$$(\partial_t + \boldsymbol{u}\cdot\boldsymbol{\nabla})\boldsymbol{u} = -\frac{1}{\rho}\boldsymbol{\nabla}p + \nu\nabla^2\boldsymbol{u} + g\alpha\theta\hat{\boldsymbol{z}},$$

$$(\partial_t + \boldsymbol{u}\cdot\boldsymbol{\nabla})\theta = \kappa\nabla^2\theta,$$

$$\boldsymbol{\nabla}\cdot\boldsymbol{u} = 0,$$

with $\boldsymbol{u}$ the velocity, p the pressure and θ the temperature fields; ρ the density, ν the kinematic viscosity, α the expansion coefficient and κ the thermal diffusivity of the fluid; and g is the acceleration due to gravity. $\hat{\boldsymbol{z}}$ is the unit vector in the upward direction. The experimental boundary conditions are

$$\boldsymbol{u} = \boldsymbol{0}, \quad \theta = 0 \quad \text{at infinity},$$
$$\boldsymbol{u} = \boldsymbol{0}, \quad \partial_r \theta = P/4\pi R^2 \kappa \rho C_p \quad \text{at the heater } (r = R),$$

where P is the power output, and where we assume that the diffusive boundary layer around the heater is isotropic. Natural units for length, time and temperature are then R, $\tau = R^2/\kappa$ and $\chi = P/R\kappa\rho C_p$ respectively. By making the change of variables we obtain

$$(\partial_t + \boldsymbol{u}\cdot\boldsymbol{\nabla})\boldsymbol{u} = -\boldsymbol{\nabla}p + \sigma\nabla^2\boldsymbol{u} + \mathscr{R}_f\theta\hat{\boldsymbol{z}},$$
$$(\partial_t + \boldsymbol{u}\cdot\boldsymbol{\nabla})\theta = \nabla^2\theta,$$
$$\boldsymbol{\nabla}\cdot\boldsymbol{u} = 0,$$

where $\sigma = \nu/\kappa$ is the Prandtl number and $\mathscr{R}_f = g\alpha P R^2/\kappa^3\rho C_p$ is a new control parameter, which we can think of as a flux Rayleigh number. $\mathscr{R}_f$ is different from the standard control parameters in two respects. First, and most important, is the fact that standard usage (dating back to Yih 1951) did not include R as a lengthscale, leaving the control parameter dependent upon powers of the height z. Second, more superficial is the third power of κ, which could be converted to a combination of powers of κ and ν by an appropriate choice of timescale, effectively a change in the σ dependence. Upon changing variables the boundary conditions change to $\partial_r\theta = 1/4\pi$ at the heater.

A different approach, well described by Batchelor (1954), supposes that we are interested only in values far away from the heater. The problem for the stem can then be solved analytically by dimensional analysis alone. This solution does not apply to the cap because it uses steady-state considerations on the conservation of heat flux. The judicious choice of unit is then to replace the power P with

$$F = (g\alpha/\rho C_p)\,P$$

which has simple dimensions (velocity)^3 × length.

We shall show experimentally that Batchelor's scaling extends to the cap once it is away from the heater. This could not be predicted beforehand, since the addition of a lengthscale to the problem can have profound effects on the solutions. The importance of the region round the heater has already been pointed out by Priestley & Ball (1955). For a complete discussion of the possible effects and scenarios once a lengthscale exists, see Barenblatt (1979, chap. 1–4).

We end up with three sets of variables for describing the scaling: Batchelor's variables, F and the viscosity ν, are simple and elegant but do not take the size of the heater R into account; then there are the non-dimensional variables $\mathscr{R}_f$ and σ, and these contain R; finally, there are the dimensional units used in the experiment. In what follows we shall give the formulae in all three forms, although the analysis is principally based on the non-dimensional units.

5. Shape of the plume

To measure the size of the plume and its scaling precisely, a model for the shape was indispensable. In a previous publication (Moses *et al.* 1991) we introduced the notion of describing the shape of the cap as a dividing line of a simple potential flow. We reported the experimental observation that the shape is well described by the Rankine

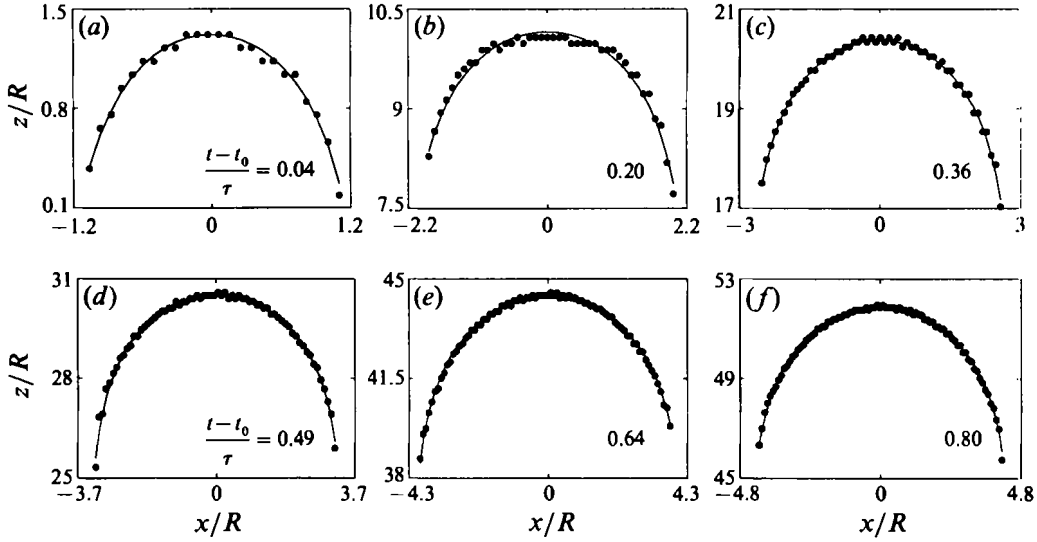

FIGURE 2. Fits of Rankine shapes to the front of a plume, $P = 1.25$ W. Dots are the digitized data and the line is the fit. Non-dimensional times t/τ and the fitted values of a/R are: (*a*) 0.16, 1.4; (*b*) 0.32, 2.3; (*c*) 0.48, 2.9; (*d*) 0.61, 3.5; (*e*) 0.76, 4.1; (*f*) 0.92, 4.6.

fairing (Rankine 1984, see also the book by Lighthill 1986 or a full description), formed by the potential flow of a point source travelling upwards in the fluid. In cylindrical coordinates, with the source at the origin and the uniform flow in the $-z$-direction, that potential is $\Phi = v_c z - J/4\pi r$, where v_c is the uniform velocity, J the strength of the source and r the distance from it. This potential is familiar from electrostatics – a charge in a uniform field. The flow defined by this potential has a stagnation point on the z-axis at $z = \frac{1}{2}a$, where $a = (J/\pi v_c)^{\frac{1}{2}}$. The streamline through this stagnation point defines a cigar-like shape of semi-infinite extent (the Rankine fairing), which is completely determined by the single parameter a, the width of the cigar quickly asymptoting to $2a$.

While potential flows have been well known for over a hundred years, their application to thermal instabilities has been rare. Use of such ideas can be found in the work of Zufiria (1988) for the Rayleigh–Taylor instability. Point singularities have also been used by Aref & Tryggvason (1989) for the Rayleigh–Taylor problem with point vortices.

In figure 2 digitized shadowgraph images of a plume similar to that of figure 1 are displayed, along with the corresponding fits to a Rankine fairing. As the plume grows in time, the parameter a grows too. The shape remains the same, reparameterized by the value of a. We have tried different forms of one-parameter models, but did not obtain a fit as good as one for the Rankine shape. It is possible by the use of two parameters to obtain a reasonable fit (to half an ellipse, for example), but a one-parameter fit is far more convincing.

Figure 3 shows a shadowgraph image of a plume under conditions similar to those of figure 1, except that the fluid is of high viscosity (500 cS) silicone oil. There are differences in size and in time scales. Everything moves more slowly in oil and the lobes do not swirl. Yet the envelope of the cap is well described by the Rankine shape for both water and oil.

While there is no rigorous justification for the model for the cap shape, once it is experimentally verified one must try to understand its plausibility. The main reason we

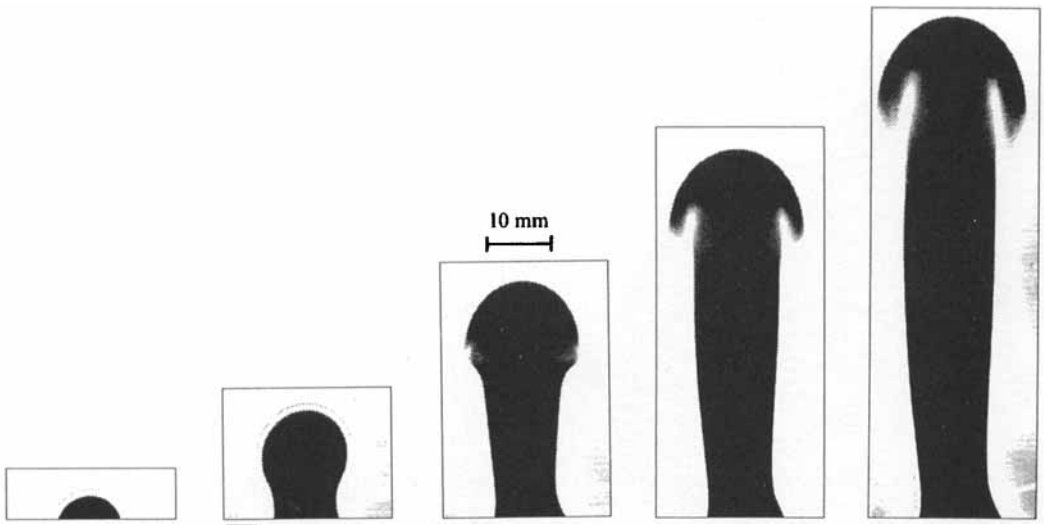

FIGURE 3. Shadowgraph images of a rising plume in 500 cS oil. $P = 1.0$ W, $R = 0.17$ cm, $t_0/\tau = 0.69$. Note that in (*a*) the plume has not erupted yet and the boundary layer is symmetric round the heater. No image subtraction was used, but a cusp in the image around the cap was eliminated digitally. Non-dimensional time t/τ is: (*a*) 0.40, (*b*) 1.04, (*c*) 1.68, (*d*) 2.32, (*e*) 2.96.

see for the success of the model comes from the experimental observation, based on the TLC studies, that the front of the plume is dominated by flow from the stem. In the frame of the cap, the jet produces an effect which is very similar to the picture given by the potential flow model. It comes from a localized source, hitting the front at a velocity $v_s - v_c$ (with v_s the stem velocity). At the same time the ambient fluid is flowing uniformly downwards.

Entrainment and vorticity occur in abundance in the lobes of the plume, but this is not necessarily so at the front. Most of the observed entrained fluid enters from the side of the cap and its lower part, playing an important role in the lobes. The outer envelope of the cap, meanwhile, is dominated by the jet impinging on the cold water above, then spreading out from the tip, subsequently descending (in the frame of the cap) to swirl and form the lobes (see insert to figure 1). This explanation is reinforced by the observation that while the plumes in low- and high-σ fluids have very different internal structure, the shape of the front is the same. It is possible that the model works because the potential flow describes the conditions outside the cap correctly.

Plumes constrained to flow in a two-dimensional channel are an interesting variation of the shape problem. Recently Zocchi, Tabeling & Ben Amar (1992) have shown that the corresponding shape is a Saffman–Taylor finger solution. They have given a theoretical treatment which explains the role of thermal diffusion in creating an interface, and which is in good agreement with their experimental measurements.

6. Results: the experimental scaling laws

6.1. *Velocity*

The easiest measurement of a plume is its height as a function of time, taking the position of the top of the cap from video data. The plumes move at a constant velocity which depends on the power input P and on fluid parameters. A large range of parameters is achieved by changing both fluids and heaters. Figure 4 shows that the

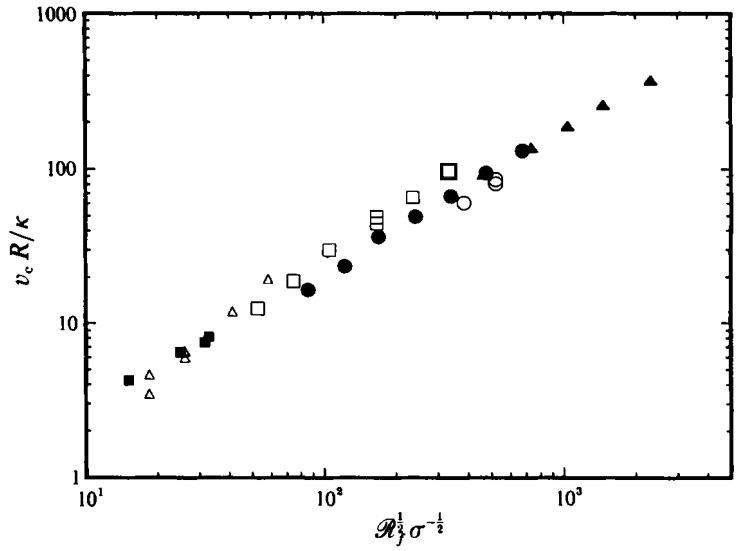

FIGURE 4. Non-dimensional velocity as function of the scaling function $\mathscr{R}_f^{\frac{1}{5}}\sigma^{-\frac{1}{2}}$: ▲, water, $R = 0.58$ cm; ●, water, $R = 0.17$ cm; ■, water, $R = 0.06$ cm; ○, methanol; □, 30 cS oil; △, 500 cS oil.

form $\mathscr{R}_f^{\frac{1}{5}}\sigma^{-\frac{1}{2}}$ describes the behaviour of v_c well. Note that this graph contains data with Reynolds number $Re = v_c a/\nu$ ranging from about 10^{-3} to about 10^2, where an instability of the cap develops. The prefactor for the relation

$$v_c = a\frac{\kappa}{R}\mathscr{R}_f^{\frac{1}{5}}\sigma^{-\frac{1}{2}} = a(F/\nu)^{\frac{1}{5}}$$

is $a = 0.23 \pm 0.05$. The error is relatively large because of the uncertainty in physical properties and because of possible non-Boussinesq effects (see discussion below). To decrease the error we put higher weight in the fit on the result for the $R = 0.17$ cm heater in water, which gives $a = 0.20 \pm 0.02$, within the previous error bar. In dimensional form we get

$$v_c = (0.2 \pm 0.02)\,(g\alpha P/\nu\rho C_p)^{\frac{1}{5}}.$$

We note one feature immediately – the heater size R has dropped out. The velocity is a quantity which can be measured at those intermediate asymptotic distances, large compared to the heater size, where we expect the heater size to be irrelevant.

While figure 4 leaves no doubt that the scaling works, the exponents derived for each fluid individually give a value of about 0.5 ± 0.1, which is a large spread. We believe this is due to non-Boussinesq effects in the silicon oils. For the temperature difference near the heater (on the order of 10 K) the viscosity changes by a factor of about 2. However, the velocity of the plume is determined by the viscosity of the fluid which is being pushed back, i.e. that of the ambient, colder fluid. Note that the result given by Shlien (1979) for water, using a totally different heating mechanism, can be described by this form to within 5%.

6.2. *Vicinity of the heater and the stem*

Phenomena that occur in the region of the heater are related to the initial formation of the plume and determine its initial conditions. These are likely to be affected by its size.

The first quantity we find is the transient time t_0 for the plume to appear, measured from when we turn on the power (see Vest & Lawson 1972 for images of the diffusive

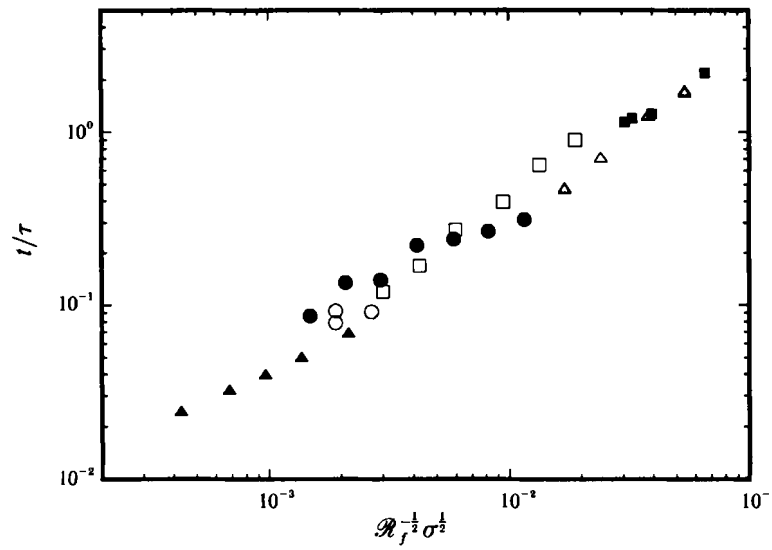

FIGURE 5. Non-dimensional build-up time t_0/τ for the plume, shown as function of the scaling relation $\mathscr{R}_f^{-\frac{1}{2}}\sigma^{\frac{1}{2}}$. Symbols as for figure 4.

boundary layer buildup). We expect the boundary layer to erupt when it reaches a critical Rayleigh number Ra_c. The time it takes to develop a diffusive boundary layer of thickness $\delta(P)$ is $t_0(P) = \delta^2/\kappa$, and we assume the boundary layer to be marginally stable to Rayleigh–Bénard convection. Another way to think of t_0 is as the time it takes for the convective transport to exceed the conduction transport in the outer part of the forming boundary layer. The latter is more physically appealing, since we know that there is no instability in the case of a horizontal gradient. However, up to a factor involving Ra_c both approaches give the same result for t_0. We write $\delta^3 = (\kappa\nu\, Ra_c)/(\alpha g \Delta)$ where Δ is the temperature at the edge of the boundary layer. The spherical diffusion profile round the heater gives a temperature $\Delta = (P\delta)/(\kappa\rho C_p R(R+\delta))$ at a distance δ from the heater. For $R > \delta$ this gives $t_0^2(P) = (Ra_c\, 4\pi R^2 \rho C_p \nu)/(P\alpha g)$, or in scaled form

$$t_0 = (4\pi\, Ra_c)^{\frac{1}{2}} \frac{R^2}{\kappa} \mathscr{R}_f^{-\frac{1}{2}} \sigma^{\frac{1}{2}} = (4\pi\, Ra_c)^{\frac{1}{2}} \left(\frac{\nu}{F}\right)^{\frac{1}{2}} R.$$

Notice that R appears in the expression for t_0. To evaluate t_0 we use the observation that for every fluid the curves of position versus time for the cap seem to originate from a common point z_0 (this is the origin of the 'virtual point source' approach, see Morton *et al.* 1956). Since $z = v_c(t - t_0)$, we can immediately evaluate t_0 from $t_0 = -z_0/v_c$. Figure 5 gives the measured values of t_0/τ as function of $\mathscr{R}_f^{-\frac{1}{2}}\sigma^{\frac{1}{2}}$ (where $\tau = R^2/\kappa$), from which we obtain $Ra_c = 130 \pm 30$. It is remarkable that this is precisely the Rayleigh number of the boundary layer in turbulent Rayleigh–Bénard convection measured both by Castaing *et al.* (1989) and by Zocchi *et al.* (1990). The value of t_0 can range from a minute or so in the 500 cS oil at 0.2 W to about a second for the same power in methanol.

It is now clear why z_0 mimics a 'virtual point source'. It is independent of power or fluid, since

$$z_0 = -v_c\, t_0 = -a \frac{\kappa}{R} \mathscr{R}_f^{\frac{1}{2}} \sigma^{-\frac{1}{2}} (4\pi\, Ra_c)^{\frac{1}{2}} \frac{R^2}{\kappa} \mathscr{R}_f^{-\frac{1}{2}} \sigma^{\frac{1}{2}} = -a(4\pi\, Ra_c)^{\frac{1}{2}} R = -(8 \pm 2)\, R.$$

Measuring z_0 thus gives a consistency check on our choice in §3 of an effective radius R for cylindrical heaters. The measured values fall within 2–4% of the calculated ones.

Other lengthscales we can measure are the stem width s, the boundary-layer thickness δ and the initial size of the plume a_0. For the stem Batchelor's scaling gives a form

$$s = \nu^{\frac{3}{4}} F^{-\frac{1}{4}} G(\sigma) z^{\frac{1}{2}},$$

with G an unknown function of the Prandtl number. We were not able, however, to establish the scaling for s experimentally. As noted in §3, the shadowgraph does not pick up the expected z-dependence, while the TLC does show a $z^{\frac{1}{2}}$ trend. Viscosity dependence could be checked only by shadowgraph measurements, since the TLC only works in water. No obvious P-dependence could be observed in either TLC or shadowgraph measurements.

The absence of any apparent P-dependence raises a problem. The hotter the stem is, the narrower it should get. We expect this dependence both from heat conservation along the stem, as in Batchelor (1954), as well as from dimensional considerations (a lengthscale other than z is needed, and we do not expect R to influence the flow away from the heater).

The situation is similar for the boundary-layer size δ, measured from the shadowgraph images. From $t_0 = \delta^2/\kappa$, and having measured the scaling for t_0, we expect to get

$$\delta = 6.3 R\mathscr{R}_f^{-\frac{1}{4}} \sigma^{\frac{1}{4}} = 6.3 \kappa^{\frac{1}{2}} \left(\frac{\nu}{F}\right)^{\frac{1}{4}} R^{\frac{1}{2}} = 6.3 \left(\frac{g\alpha P}{\kappa \nu^2 \rho C_p}\right)^{-\frac{1}{4}} R^{\frac{1}{2}}.$$

The measured values for δ are 0.05, 0.08, 0.12, 0.09, 0.26 and 0.48 cm for $R = 0.06$, 0.17 and 0.58 cm in water, and $R = 0.17$ cm in methanol, 30 cS oil and 500 cS oil, respectively. There are four data points covering three orders of magnitude in ν, which are consistent with a $\frac{1}{4}$-power law. Three data points for R, covering one order of magnitude, are consistent with an $R^{\frac{1}{2}}$ behaviour. The range covered in P was slightly less than two orders of magnitude, but the narrowing with P was not apparent.

The measured values (from the shadowgraph) for a_0, which determines the initial size of the stem, were 0.08, 0.16, 0.28, 0.12, 0.5 and 0.8 cm for $R = 0.06$, 0.17 and 0.58 cm in water, and $R = 0.17$ cm in methanol, 30 cS oil and 500 cS oil, respectively. As for the δ measurements, the four data points for ν are well described by a $\nu^{\frac{1}{4}}$ behaviour, and the three data points for R are well described by an $R^{\frac{1}{2}}$ behaviour. No apparent P-dependence was observed here either.

We see no clear theoretical consideration which would explain the absence of an apparent P-dependence, and tend to view it as an artifact of the measuring techniques. The effect of changing P by two orders of magnitude (one order of magnitude for the TLC measurements) is expected to be a factor of $100^{\frac{1}{4}} \sim 3.2$ ($10^{\frac{1}{4}} \sim 1.8$ for the TLC), which is not large. As the shadowgraph does not show the widening of the stem with z, possibly neither it nor the TLC show the effect of power on the stem and the boundary layer. Shlien & Boxman (1979) have shown that the temperature profile at a given height in the stem is Gaussian. As the stem becomes hotter, more of the profile's extent can be seen by the shadowgraph. It is possible that the narrowing of the Gaussian profile is compensated by the higher temperatures inside it, leaving the region that is within the sensitivity of our measuring techniques practically unchanged.

6.3. *Cap width*

Batchelor's scaling predicts a parabolic profile for the stem size $s \sim z^{\frac{1}{2}}$, and we checked experimentally that this extends to the cap size a. To cast this in the form of a diffusion process we introduce time, using the linear relation $z = v_c(t - t_0)$.

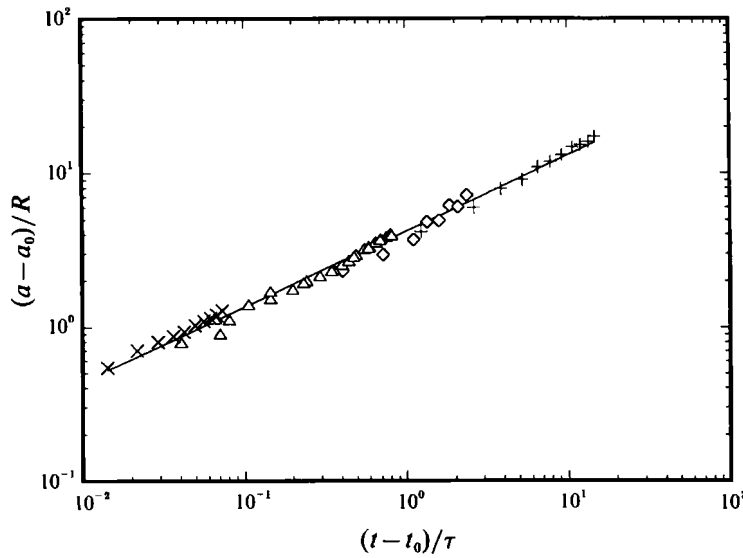

FIGURE 6. Size of the cap as function of time. The width is obtained from the fit to a Rankine fairing. a_0 and t_0 are initial conditions. The fluid is water. +, $R = 0.06$ cm, $P = 0.08$ W; ◇, $R = 0.17$ cm, $P = 0.08$ W; △, $R = 0.17$ cm, $P = 1.25$ W; ×, $R = 0.58$ cm, $P = 1.26$ W.

No exponent can reliably be extracted experimentally from a single plume, so we accumulated statistics on short times from fast, well-defined plumes and on long times from slow plumes. For faint plumes we were greatly aided by the fitting procedure for the Rankine shape, extrapolating a width from the curvature at the tip. This leads to some scatter in the measured values of a. When the plume protrudes out of the boundary layer, its cap is already formed. We used the values measured in §6.2 above for this initial size a_0.

The $\mathscr{R}_f$ dependence was first examined by looking at $(a-a_0)/R$ as a function of time in water for several different powers, ranging over almost two decades in $\mathscr{R}_f$. No dependence on $\mathscr{R}_f$ was observed. Least-squares fitting to the form $a-a_0 = d[\kappa(t-t_0)]^\beta$ gave an exponent of 0.54 ± 0.05. The dependence on time (or on height) is indeed diffusive. R disappears from the expression, as expected for measurements far enough from the heater.

As time is scaled by $\tau = R^2/\kappa$, we can extend our range by using very small as well as very large heaters. In figure 6 three different heaters are compared in water. We used cylinders of effective radius 0.06, 0.17 and 0.58 cm. The slope is very close to $\frac{1}{2}$ (actual best fit is to an exponent of 0.49). To find the dependence on the Prandtl number we also looked at the cap size $(a-a_0)/R$ as a function of time for the four different fluids. We found that the growth does not depend on viscosity, and fitting the data to the form $a-a_0 = d[\kappa(t-t_0)]^\beta$ we find again $\beta = 0.49$ and $d = 4.1$. We summarize that $d = 4.2 \pm 0.2$, giving an effective diffusion-constant value $\kappa' = (17.5 \pm 3)\kappa$. In terms of the scaling parameters

$$a-a_0 = (4.2 \pm 0.2)\, R\left(\frac{t-t_0}{\tau}\right)^{\frac{1}{2}} = (4.2 \pm 0.2)\, \sigma^{-\frac{1}{2}}\left(\frac{\nu^3}{F}\right)^{\frac{1}{4}} z^{\frac{1}{2}}.$$

The fact that $\kappa' \gg \kappa$ indicates that the process is not a molecular one. This is an enhanced diffusion process, aided by advection and entrainment, 17.5 times stronger than that of purely thermal diffusion. R is eliminated by the $\tau^{\frac{1}{2}}$-dependence.

To summarize, we found that the growth of the cap of the plume is determined by an enhanced thermal diffusive process. Surprisingly, the velocity of the cap can have an effect only indirectly, through this enhancement, in which entrainment must play a role.

6.4. *Cap temperature*

The point-source scaling given by Batchelor predicts for the temperature $\theta \sim F/\nu z$, which implies a constant Nusselt number Nu, independent of $\mathscr{R}_f$ (or F). This contradicts our notion that the efficiency of cooling the heater is enhanced by the flow. Near the heater a circulating flow exists, a large-scale flow that brings in cooler fluid and injects it into the stem. The point-source scaling does not take this into account and, as usual, near the heater we can expect it to fail. Thus we can scale three different temperatures: the heater, the stem and the cap. We shall not treat the stem here, but see Shlien & Boxman (1979).

We first look at the scaling of the temperature measured inside the heater. Writing as usual $\theta = \mathscr{R}_f^{\alpha}\sigma^{\beta}f(t/\tau, z/R \ldots)$ we found first by comparing water and the oils that viscosity plays no role in determining θ, so that $\beta = 0$. The $\mathscr{R}_f$ dependence of the temperature θ inside the heater for water and the oils is well described by a power law with exponent $\alpha = -0.12 \pm 0.03$, which, since θ is scaled by P, translates into

$$Nu \sim \mathscr{R}_f^{0.12}$$

at the heater. The prefactor depends on the exact location of our probe inside the heater, and is irrelevant. Note that it is hard to pinpoint small exponents, and we may be seeing a logarithmic correction to scaling.

Putting a thermistor in the path of the plume gives a picture of its temperature distribution. The temperature climbs rapidly as the cap strikes the thermistor, peaking at a distance from the front which is comparable to the cap width a. It then relaxes to a steady-state value about 15% lower in the stem. This signature of the plume occurs for all the fluids we used, but is more stable for the viscous oils. The peak in the cap, or 'transient' of the stem was noticed by Shlien & Boxman (1979, 1981), and is intriguing when one remembers that the stem is the source for the cap. Presumably a blob of fluid loses more heat along the stem than while passing through the 'thermal insulation' provided by the cap. The plume stem and cap then scale similarly but with slightly different prefactors.

Using the peak as a measure of the cap temperature we can find the scaling in the cap. It is different than the scaling of the heater's temperature in that the $\mathscr{R}_f$ dependence is barely visible. While a fit to a power law gives $\alpha = -0.04 \pm 0.03$, the data is indistinguishable from a constant.

We turn to the behaviour of θ with height, and find that it tends to $1/z$ for z/R greater than about 10. Below that value no power-law behaviour was observed. Figure 7 gives the z/R dependence of θ for water and the oils. We cannot obtain a large scaling range by changing heater size, because the temperature scaling with R compensates for the scaling of z with R. The slope is close to unity (actual value of the best fit to a power law is 0.91). Similar deviations exist in the work on the stem by Shlien (1979) – he used an offset to a 'virtual source' to get a $1/z$ dependence, while Schorr & Gebhart (1970) report effects of the finite size of the heater for a line source.

We summarize our results away from the heater by

$$\theta = (0.05 \pm 0.01)\,\chi\frac{R}{z} = (0.05 \pm 0.01)\,\sigma\frac{F}{g\alpha\nu}z^{-1} = (0.05 \pm 0.01)\frac{P}{\kappa\rho C_p}z^{-1},$$

where $\chi = P/R\kappa\rho C_p$ and $F = Pg\alpha/\rho C_p$.

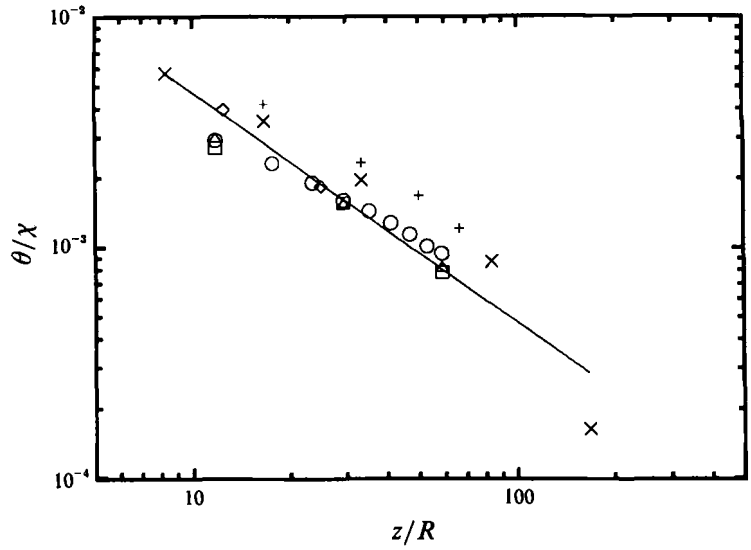

FIGURE 7. Non-dimensional temperature as function of height from heater for various values of R and of $\mathscr{R}_f$ in water and oil. ○, 500 cS, oil, $R = 0.17$ cm, $P = 0.5$ W; +, 500 cS oil, $R = 0.06$ cm (various powers); ◇, water, $R = 0.4$ cm sphere, $P = 0.5$ W; □, water, $R = 0.17$ cm, $P = 0.5$ W; △, water, $R = 0.17$ cm, $P = 0.2$ W; ×, water $R = 0.6$ cm (various powers).

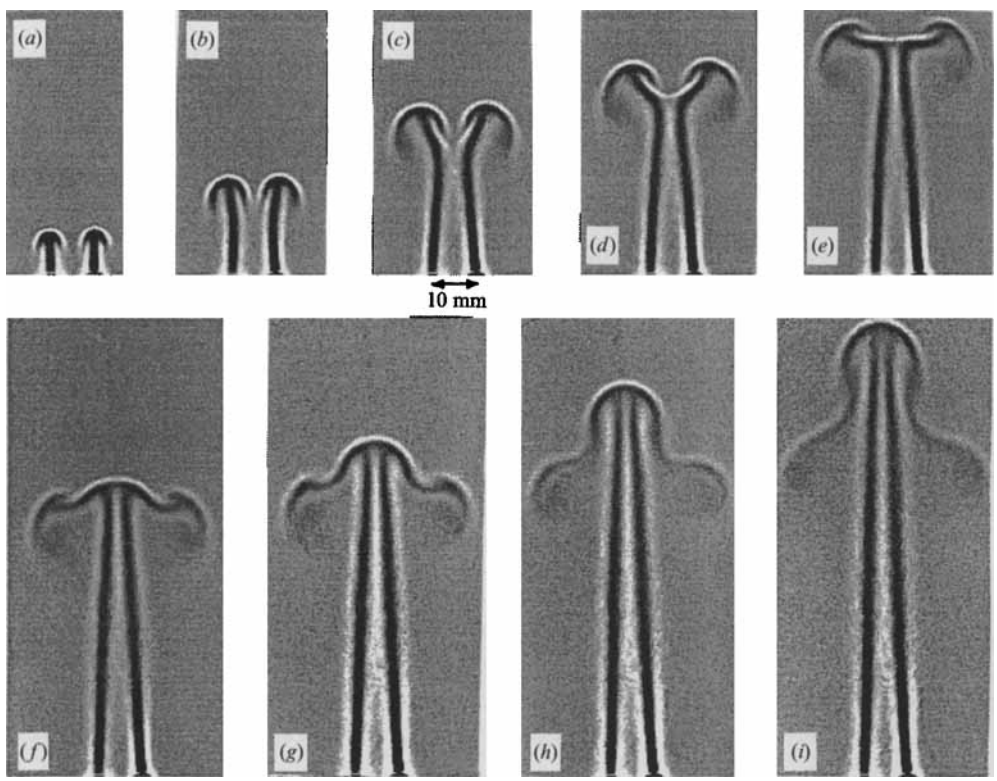

FIGURE 8. Interaction between two neighbouring plumes in water. The distance between the two $R = 0.17$ cm heaters is $d_0/R = 5.3$, $P = 0.25$ W per heater and $t_0/\tau = 0.26$. Non-dimensional time t/τ is: (*a*) 0.48, (*b*) 0.73, (*c*) 1.07, (*d*) 1.28, (*e*) 1.50, (*f*) 1.71, (*g*) 1.83, (*h*) 2.02, (*i*) 2.21.

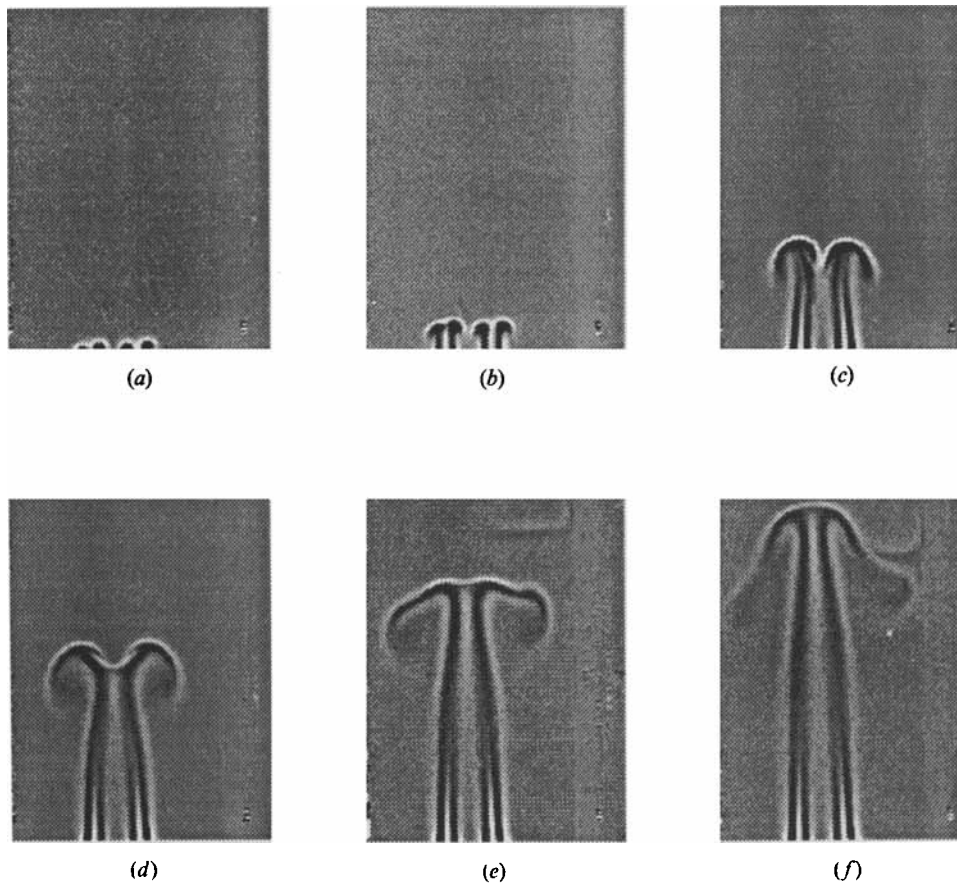

FIGURE 9. Multiple interactions, leading from four independent, collinear plumes to one joint cap with four stems. The field of view covers 87×65 mm^2. Heaters (not in the picture) are of size $R = 0.17$ cm, $P = 0.51$ W per plume, and $t_0/\tau = 0.18$. Non-dimensional time from switching on of power t/τ is: (*a*) 0.45, (*b*) 0.60, (*c*) 1.02, (*d*) 1.51, (*e*) 1.96, (*f*) 2.34.

7. More than one plume

Plumes interact, collide, etc. The interaction between two plumes is shown in figure 8, and has been studied in more detail in Moses *et al.* (1991), where it was shown that the model of sources and sinks describes the velocity field of two plumes, and can reconstruct the interaction between them up to the point (figure 8*d*) beyond which the plumes join to form one unified object.

To obtain a criterion for coalescence of two nearby plumes, we estimate the height z_c at which two plumes from heaters at a distance d_0 will coalesce as the height at which $a = d_0$. We get

$$d_0 = (4.2 \pm 0.2)\,\sigma^{-\frac{1}{2}} \left(\frac{\nu^3}{F}\right)^{\frac{1}{4}} z_c^{\frac{1}{2}}, \quad \text{or} \quad z_c = 0.06\sigma \left(\frac{F}{\nu^3}\right)^{\frac{1}{2}} d_0^2.$$

The possibility of an inverse cascade comes to mind, and we show in figure 9 how four plumes, arranged collinearly to interact first in pairs, change from four (figure 9*a*) to two (figure 9*c*) to one (figure 9*f*) caps. If we put a power P into each of the four single plumes, their velocity is equal and proportional to $P^{\frac{1}{3}}$. Once the first interaction

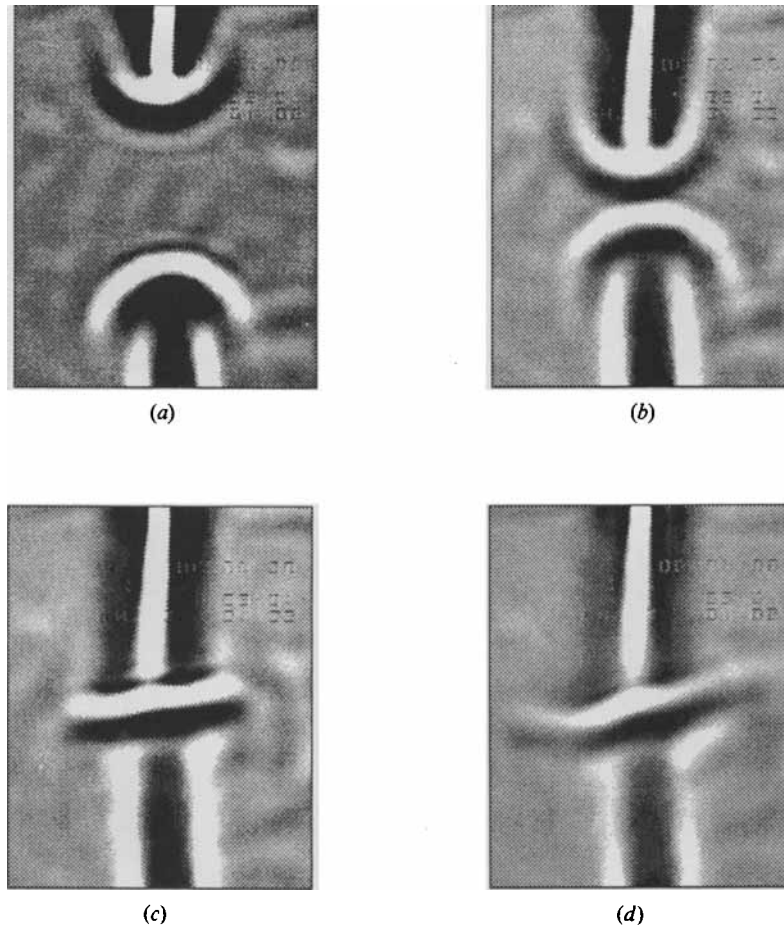

FIGURE 10. Collision of a hot and cold equal-power plume pair. Time between frames is 3 s (dimensional – since the effective radius of the Peltier element is undetermined).

process is complete, the two caps rise at a velocity of $\sqrt{2}P^{\frac{1}{2}}$. After the next interaction the velocity goes up again, with the final velocity of the single cap proportional to $2P^{\frac{1}{2}}$. During the interaction stage the velocity drops temporarily.

In figures 10 and 11 we present head-on interactions of hot and cold counter-propagating plumes. The cold plume was produced by a small Peltier element. The strength of both plumes was adjusted so that the collision was symmetric. Figure 10 shows the collision between a cold (white) and hot (dark) plume. As they collide the caps flatten out, making a circular disc with an interesting vertical structure. The boundary between the colliding plumes is sharp, and is maintained for some time. The two plumes retain their identity, and there is no mixing or coalescence as is observed with 'like-sign' plumes.

It is actually hard to get the plumes to collide head-on (impact parameter 0) although figure 10 is close to that. Usually the two plumes would hit at non-zero impact parameter, and sometimes would enter into a 'bound state', rotating around a common centre. This is shown in figure 11, which is a state of two plumes that rotate around each other, alternately forming a front and deflecting off each other. This state was observed for over 20 min, with the period stable over short times (10–20 cycles), but drifting randomly between 15 and 25 s over longer times. The process resembles a

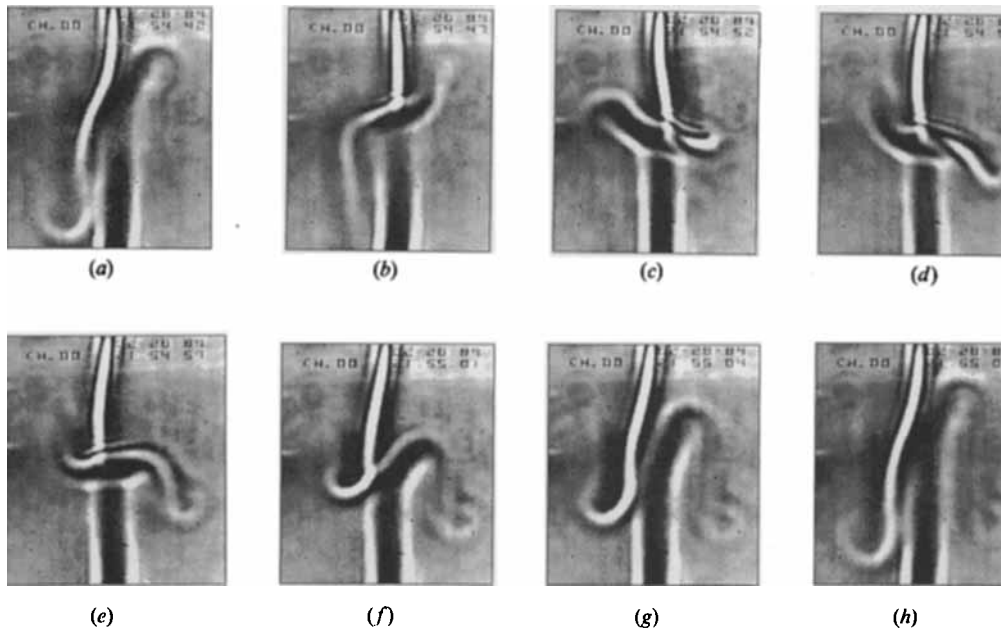

FIGURE 11. 'Bound state' of cold and hot plumes rotating round each other, periodically forming a front and then parting to emit a cap in each direction. Time is: (*a*) $t = 0$, (*b*) 5 s, (*c*) 10 s, (*d*) 15 s, (*e*) 17 s, (*f*) 19 s, (*g*) 22 s, (*h*) 25 s.

state of two orbiting particles that emit energy once every cycle – this is the cap of the plumes that is shed when the front is re-formed (bottom right in figure 11*e–h*).

8. Plumes in turbulence

It is natural to assume that plumes which appear in turbulent convection would be turbulent as well. We were therefore surprised to find the situation shown in figure 12. We show here the shadowgraph of a part of a cubic ($18.5 \times 18.5 \times 18.5$ cm^3) convection cell with water at $Ra \sim 10^9$ and $\sigma = 6$, close to the region of turbulence defined by Heslot, Castaing & Libchaber (1987) as 'hard turbulence'. In brief, Zocchi *et al.* (1990) found that the large-scale flow is directed along the diagonal in the box. Plumes are ejected from ripples (or 'waves') of the (say bottom, or hot) thermal boundary layer, and swept by the large-scale wind towards the corners, where they tend to accumulate. There they climb up, strike the top thermal boundary layer, exciting a new wave, which will eject new plumes, which continues the cycle. We note in passing that coalescence of two plumes climbing together often occurs, while collisions occur at the off-diagonal corners, where both upward and downward plumes can appear.

Figure 12 shows the centre section of the bottom half of the cell, and the field of view is about 5×7 cm. The shadowgraph averages along the width of the cell, so the plumes we see do not overlap: they are at different distances in the third dimension. We focus on one plume, marked by an arrow in figure 12(*a*), and follow it. It is lightly atypical because it does not reach the corner, but that is why we chose it, so that we can follow it alone. We did check that the plumes in the corner are similar in shape and behaviour. We note three things: first, the source of the plume is localized; secondly, the rising velocity is constant; thirdly, the shape of our plume is not distorted over the first fourth of its journey to the top, in fact it resembles the isolated plumes we have studied in a quiescent background.

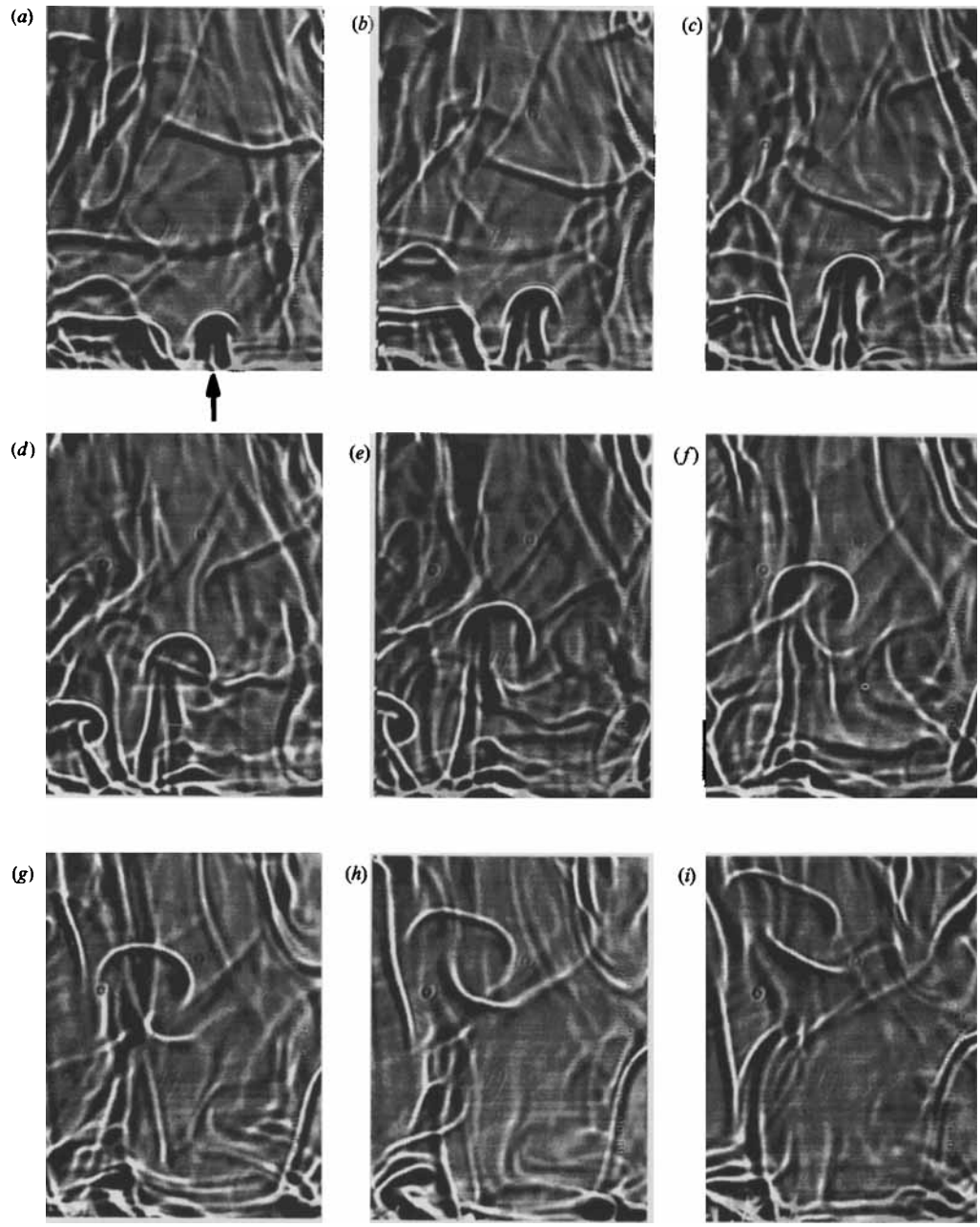

FIGURE 12. Shadowgraph images of the turbulent cell at $Ra \sim 10^9$. The arrow marks the plume under study. Field of view is about 7×5 cm^2 through the centre of the bottom half of the cell. Time is: (*a*) $t = 0$, (*b*) 0.9 *s*, (*c*) 1.9 s, (*d*) 3.0 s, (*e*) 4.0 s, (*f*) 5.1 s, (*g*) 6.1 s, (*h*) 7.2 s, (*i*) 8.2 s.

To verify that these plumes are indeed like the laminar plumes we have studied, we show in figure 13 the digitized interface, along with a fit to a Rankine shape. The fit is good until $t = 4$ s, which corresponds to figure 12(*e*). Beyond that time the plume loses its Rankine form by being stretched, distorted by the surrounding flow. Shlien (1978) showed that an unstable plume solution looks very different. The instability of

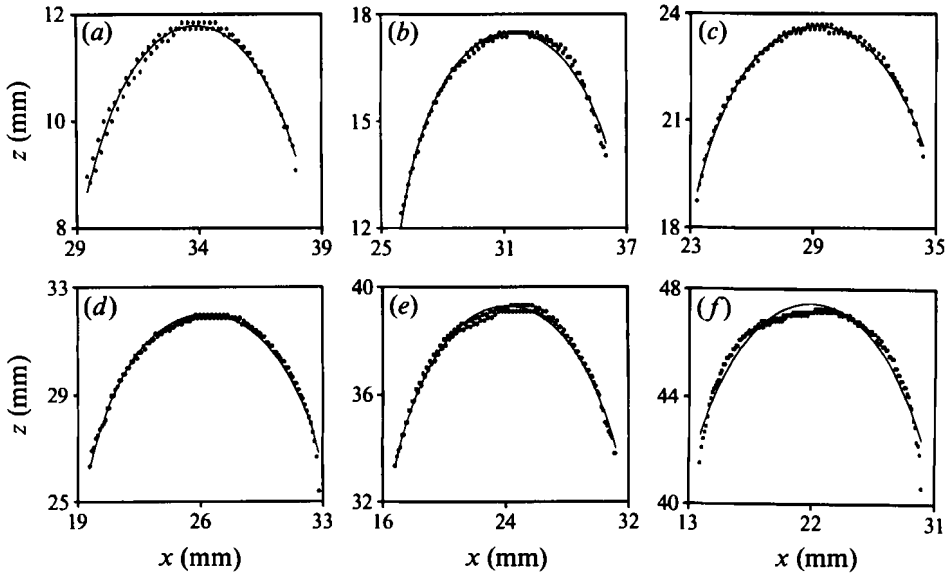

FIGURE 13. Digitized front of the plume marked in figure 12(*a*). Dots are data, and the line is a fit to the Rankine shape. Fitted values of a are: (*a*) 8.5 mm, (*b*) 8.9 mm, (*c*) 10.5 mm, (*d*) 11.5 mm, (*e*) 13.0 mm, (*f*) 16.7 mm. Time is: (*a*) $t = 0$, (*b*) 0.9 s, (*c*) 1.9 s, (*d*) 30 s, (*e*) 4.0 s, (*f*) 5.1 s.

the cap is a spiralling mode, while the stem has a wavy instability. The cap first tilts one way, then begins to spiral round the stem, which pushes beyond it and leaves it behind, creating a new cap, to be subsequently shed also. Shlien also measured the Reynolds number for the size of the cap at the transition to be about 200. Thus the plume itself is not turbulent at $Ra \sim 10^9$ and $\sigma = 6$. Using our scaling and the measured cap velocity ($v_c = 0.69$ cm/s) we can calculate the power input into the plume to be $P = 1.7$ W. The total power put into the cell in this state is about 60 W.

The turbulent behaviour of the convection at $Ra \sim 10^9$ and $\sigma = 6$ is probably due to the interaction of many laminar plumes and the large-scale 'wind', not due to turbulence in the individual plume. We can expect that at higher Ra the plumes will destabilize and lead to new regimes, as discussed in Procaccia *et al.* (1991). We know from our scaling that in fluids of smaller viscosity (e.g. helium at low temperatures – see Castaing *et al.* 1989) the instability develops earlier, so the plumes there may already be turbulent at these Rayleigh numbers.

9. Conclusions

Most of the relevant scalings have been established. While vorticity has not been measured, the fact that the potential flow approach to the plume shape works indicates that this measurement may not be essential. Furthermore, the large scaling range we have with σ (and Re) indicates that for the very slow, essentially structureless plumes in oil, as well as the plumes with large vorticity in methanol and water, the common features are those which disregard their vorticity content. We have formulated the scaling hypothesis in variables which take into account the finite size of the heater ($\mathscr{R}_f = g\alpha PR^2/\kappa^3\rho C_p$, and $\sigma = \nu/\kappa$), and checked that this is consistent at large distances with Batchelor's point-source scaling for the stem (using the variables $F = g\alpha P/\rho C_p$ and ν).

Our experimental measurements have shown that:

(i) the rising velocity of the plume is constant, depends on the square root of the non-dimensionalized power, and is inversely proportional to the square root of the viscosity ν (figure 4);

(ii) the width of the cap grows by an enhanced thermal diffusion process (figure 6);

(iii) the temperature has a linear dependence on power, no dependence on the control parameters, and is inversely proportional to height (figure 7), surprisingly like a diffusive profile.

Interactions between plumes can be understood in terms of simple dynamics of single excitations. We have further found that plumes in some range of turbulent convection can be described by the above scaling.

We thank B. Shraiman, S. Zaleski, L. Kadanoff and I. Procaccia for useful discussions, and B. Berge, A. Simon, and X. Z. Wu for experimental advice. This work was supported by the NSF under grants DMR 8722714 and MRL 8819860.

REFERENCES

AREF, H. & TRYGGVASON, G. 1989 Model of Rayleigh Taylor instability. *Phys. Rev. Lett.* **62**, 749–752.

BARENBLATT, G. I. 1979 *Similarity, Self Similarity and Intermediate Asymptotics* (translated by N. Stein; ed. M. Van Dyke). Plenum.

BATCHELOR, G. K. 1954 Heat convection and buoyancy effects in fluids. *Q. J. R. Met. Soc.* **80**, 339–358.

CASTAING, B., GUNARATNE, G., HESLOT, F., KADANOFF, L., LIBCHABER, A., THOMAE, S., WU, X. Z., ZALESKI, S. & ZANETTI, G. 1989 Scaling of hard thermal turbulence in Rayleigh–Bénard convection. *J. Fluid Mech.* **204**, 1–30.

CHU, T. Y. & GOLDSTEIN, J. R. 1973 Turbulent convection in a horizontal layer of water. *J. Fluid Mech.* **60**, 141–159.

FUJII, T. 1963 Theory of the steady laminar natural convection above a horizontal line heat source and a point heat source. *Intl J. Heat Mass Transfer* **6**, 597–606.

FUJII, T., MORIOKA, I. & UEHARA, U. 1973 Buoyant plume above a horizontal line heat source. *Intl J. Heat Mass Transfer* **16**, 755–768.

GEBHART, B., JALURIA, Y., MAHANJAN, R. L. & SAMMAKIA, B. 1988 *Buoyancy Induced Flows and Transport*. Hemisphere.

GEBHART, B., PERA, L., SCHORR, A. W. 1970 Steady laminar natural convection plumes above a horizontal line heat source. *Intl J. Heat Mass Transfer* **13**, 161–171.

HESLOT, F., CASTAING, B. & LIBCHABER, A. 1987 Transition to turbulence in helium gas. *Phys. Rev.* A **36**, 5870–5873.

LIGHTHILL, M. J. 1986 *An Informal Introduction to Theoretical Fluid Mechanics*. Oxford University Press.

MORTON, B. R., TAYLOR, G. I. & TURNER, J. S. 1956 Turbulent gravitational convection form maintained and instantaneous sources. *Proc. R. Soc. Lond.* A **234**, 1–23.

MOSES, E., ZOCCHI, G., PROCACCIA, I. & LIBCHABER, A. 1991 The dynamics and interaction of laminar thermal plumes. *Europhys. Lett.* **14**, 55–60.

NEUMANN, J. VON 1941 *NDRC, Div. B, Rep.* AM-9, June 30, 1941.

NEUMANN, J. VON 1947 The point source solution. *Los Alamos Rep.* LA-2000, pp. 27–55.

PERA, L. & GEBHART, G. 1971 On the stability of laminar plumes: some numerical solutions and experiments. *Intl J. Heat Mass Transfer* **14**, 975–984.

PERA, L. & GEBHART, B. 1975 Laminar plume interactions. *J. Fluid Mech.* **68**, 259–271.

POLYMEROPOULOS, C. E. & GEBHART, B. 1967 Incipient instability in free convection laminar boundary layers. *J. Fluid Mech.* **30**, 225–239.

PRIESTLEY, C. H. B. & BALL, F. K. 1955 Continuous convection from an isolated source of heat. *Q. J. R. Met. Soc.* **81**, 144–157.

PROCACCIA, I., CHING, E., CONSTANTIN, P., KADANOFF, L. P., LIBCHABER, A. & WU, X. Z. 1991 Transitions in convective turbulence: the role of thermal plumes. *Phys. Rev.* A **44**, 8091–8102.

RANKINE, W. J. M. 1964 On plane water lines. *Phil. Trans. R. Soc. Lond.* A **154**, 369–391.

SCHORR, A. W. & GEBHART, B. 1970 An experimental investigation of natural convection wake above a line heat source. *Intl J. Heat Mass Transfer* **13**, 557–571.

SHLIEN, D. J. 1976 Some laminar thermal and plume experiments. *Phys. Fluids* **19**, 1089–1098.

SHLIEN, D. J. 1978 Transition of the axisymmetric starting plume cap. *Phys. Fluids* **21**, 2154–2158.

SHLIEN, D. J. 1979 Relations between point sources buoyant convection phenomena. *Phys. Fluids* **22**, 2277–2283.

SHLIEN, D. J. & BOXMAN, R. L. 1979 Temperature field measurement of an axisymmetric laminar plume. *Phys. Fluids* **22**, 631–634.

SHLIEN, D. J. & BOXMAN, R. L. 1981 Laminar starting plume temperature field measurement. *Intl J. Heat Mass Transfer* **24**, 919–930.

SHLIEN, D. J. & BROSH, A. 1979 Velocity field measurements of a laminar thermal. *Phys. Fluids* **22**, 1044–1053.

SOLOMON, T. H. & GOLLUB, J. P. 1990 Sheared boundary layers in turbulent Rayleigh–Bénard convection. *Phys. Rev. Lett.* **64**, 2382–2385.

SPARROW, E. M., HUSAR, R. B. & GOLDSTEIN, J. R. 1970 Observations and other characteristics of thermals. *J. Fluid Mech.* **41**, 793–806.

TAYLOR, G. I. 1941 *British Rep.* RC-210, June 27, 1941.

TAYLOR, G. I. 1950*a* The formation of a blast wave by a very intense explosion. I. Theoretical discussion. *Proc. R. Soc. Lond.* A **201**, 159–174.

TAYLOR, G. I. 1950*b* The formation of a blast wave by a very intense explosion. II. The atomic explosion of 1945. *Proc. R. Soc. Lond.* A **201**, 175–186.

TURNER, J. S. 1962 The starting plume in neutral surroundings. *J. Fluid Mech.* **13**, 356–368.

TURNER, J. S. 1969 Buoyant thermals and plumes. *Ann. Rev. Fluid Mech.* **1**, 29–44.

TURNER, J. S. 1973 *Buoyancy Effects in Fluids.* Cambridge University Press.

TURNER, J. S. 1986 Turbulent entrainment: the development of the entrainment assumption, and its application to geophysical flows. *J. Fluid Mech.* **173**, 431–471.

VEST, C. M. & LAWSON, M. L. 1972 Onset of convection near a suddenly heated horizontal wire. *Intl J. Heat Mass Transfer* **15**, 1281–1283.

YIH, C. S. 1951 Free convection due to a point source of heat. In *Proc. First US Natl Cong. Appl. Mech.*, pp. 941–947.

ZELDOVICH, YA. B. 1937 Limiting laws of freely rising convection currents. *Zh. Eksp. Teor. Fiz.* **7**, 1463–1465.

ZOCCHI, G., MOSES, E. & LIBCHABER, A. 1990 Coherent structures in turbulent convection, an experimental study. *Physica* A **166**, 387–407.

ZOCCHI, G., TABELING, P. & BEN AMAR, M. 1992 Saffman Taylor plumes. *Phys. Rev. Lett.* **69**, 601–604.

ZUFIRIA, J. 1988 Bubble competition in Rayleigh Taylor instability. *Phys. Fluids* **31**, 440–446.